Acta Crystallographica Section B
Structural Science
ISSN 0108-7681

New RE microporous heteropolyhedral silicates containing $4^1 5^1 6^1 8^2$ tetrahedral sheets

Marcella Cadoni,[a,b] Yan Ling Cheah[a,c] and Giovanni Ferraris[a,b]*

[a]Dipartimento di Scienze Mineralogiche e Petrologiche, Università di Torino, Via Valperga Caluso 35, I-10125, Torino, Italy, [b]Nanostructured Interfaces and Surfaces (NIS) Centre of Excellence – Via Pietro Giuria 7, I-10125 Torino, Italy, and [c]School of Materials Science and Engineering, Nanyang Technological University, N4.1-B4-10, 50 Nanyang Avenue, Singapore 639798, Singapore

Correspondence e-mail: giovanni.ferraris@unito.it

Received 13 November 2009
Accepted 24 December 2009

Four heteropolyhedral microporous silicates, $A_3RESi_6O_{15}\cdot 2.25H_2O$, crystallizing in the *Cmm*2 space group and based on $4^1 5^1 6^1 8^2$ tetrahedral sheets [$A_3 = Na_{2.74}K_{0.26}$, RE = Ce, abbreviated as TR05; TR06: $A_3 = Na_{2.72}K_{0.28}$, RE = La; TR07: $A_3 = Na_3$, RE = La; TR08: $A_3 = Na_{2.74}(H_3O)_{0.26}$, RE = $La_{0.68}Eu_{0.32}$] have been hydrothermally synthesized in Teflon-lined autoclaves at 503 K and structurally characterized using X-ray diffraction single-crystal data. Except for TR05, diffraction data have been collected on {001} twins by merohedry. The four structures are isotypic and based on strongly corrugated $4^1 5^1 6^1 8^2$ silicate sheets interconnected along [010] by seven-coordinated RE polyhedra to form a microporous heteropolyhedral framework. The framework is crossed by three systems of ellipsoidal channels that host H_2O molecules and alkaline ions. The channels run either parallel or perpendicular to the silicate sheets; the largest effective channel width is 4.7×2 Å. In TR08 some $(H_3O)^+$ replaces alkalis. Although the H atoms have not been localized, the configuration of the hydrogen bonding has been deduced from bond lengths and angles.

1. Introduction

Krivovichev (2009) defines 'a *ring symbol* as a sequence $p_1^{r_1} p_2^{r_2} \ldots p_n^{r_n}$, where $p_1, p_2 \ldots p_n$ are numbers of nodes in a ring and r_1, $r_2 \ldots$ r_n are relative numbers of the corresponding rings in a graph'. In this article the nodes of the graph represent silicate tetrahedra and the corresponding two-dimensional sheet is not necessarily strictly planar. Some geometrical aspects of this type of silicate sheet had already been analysed by Liebau (1985) and Haile & Wuensch (1997) who emphasized the presence of wollastonite-type chains that condense to form xonotlite-like double chains containing eight-rings. The condensation of the double chains leads to $p_1^{r_1} p_2^{r_2} \ldots p_n^{r_n}$ sheets. Liebau (1985) introduced a detailed nomenclature to classify the tetrahedral sheets, in particular naming tertiary, quaternary and non-tertiary those tetrahedra sharing three, four and less than three vertices. The most common $p_1^{r_1} p_2^{r_2} \ldots p_n^{r_n}$ silicate sheet is 6^1 that occurs in layered silicates like micas, where all tetrahedra are pointing in one direction being generated by the periodic repetition of a pyroxene-like chain. Mixed up- (u) and down-pointing (d) tetrahedra allow the formation of geometrical isomers that can be classified by coupling a sequence of us and ds with a ring symbol.

In the tetrahedral sheets described here the T central atom of a tetrahedron is Si, that may be replaced by Al, and the vertices are occupied by O atoms, in some cases belonging to OH groups. If only tertiary tetrahedra occur T/O = 2/5, as in

micas and in the compounds described in this article; the presence of non-tertiary tetrahedra implies T/O < 2/5 (*e.g.* $K_7Ln_3[Si_{12}O_{32}]\cdot xH_2O$; Ananias *et al.*, 2009); finally, quaternary tetrahedra require T/O > 2/5 and, more importantly, the sheet must be either branched (*e.g.* meliphanite; Grice & Hawthorne, 2002) or doubled to form microporous layers, as in the rhodesite series (Cadoni & Ferraris, 2009, 2010, and references therein). Some $p_1^{r_1}p_2^{r_2}\ldots p_n^{r_n}$ silicate sheets are shown in Fig. 1 (all figures of structures by *ATOMS*; Dowty, 2002). The sheets can constitute building modules either of *s.s.* layered structures, where the strong bonds are confined within layers that are interconnected by weak bonds (typically phyllosilicates), or of heteropolyhedral frameworks. The latter are obtained when the silicate sheets are interconnected by strong bonds *via* five-, six- or seven-coordinated polyhedra and are often crossed by channels.

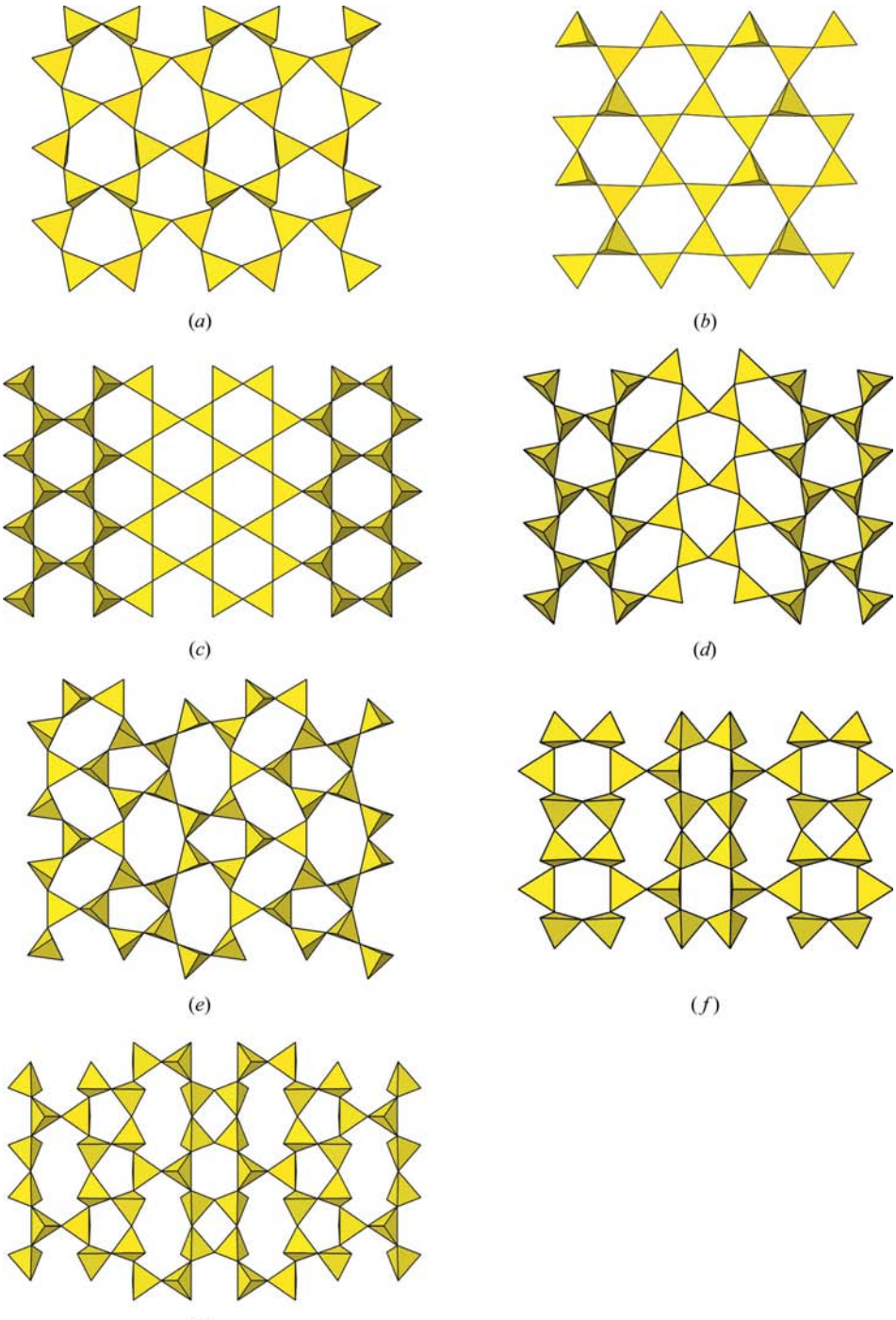

Figure 1
Examples of $p_1^{r_1}p_2^{r_2}\ldots p_n^{r_n}$ tetrahedral sheets. 6^1 sheet as part of a double layer in the heteropolyhedral structures of $Rb_2Cu_2[Si_8O_{19}]$ (Watanabe & Kawahara, 1993) (*a*) and (*b*) of $Rb_2(VO)_2[Si_8O_{19}]$ (Prinz *et al.*, 2008); 6^1 sheet as part of a microporous tetrahedral framework in the palysepioles (Ferraris *et al.*, 1998) (*c*) sepiolite ($Mg_8[Si_{12}O_{30}](OH)_4\cdot 12H_2O$; Brauner & Preisinger, 1956) and (*d*) palygorskite ($Mg_5[Si_8O_{20}](OH)_2\cdot 8H_2O$; Artioli & Galli, 1994); (*e*) $5^16^27^1$ sheet as part of a double layer in the heteropolyhedral structure of $Na_4[Cu_2Si_{12}O_{27}(OH)_2][(NaOH)_2(H_2O)_6]$ (Wang *et al.*, 2003); (*f*) $4^16^18^1$ sheet occurring in sazhinite-(La) ($Na_3LaSi_6O_{15}\cdot 2H_2O$; Càmara *et al.*, 2006); (*g*) $4^15^16^18^2$ sheet (this work).

Heteropolyhedral microporous structures are modular structures (Ferraris *et al.*, 2008) and those occurring in the mineral realm (Ferraris & Merlino, 2005) often were the incentive for the synthesis of new compounds suitable for technological applications (*e.g.* ion exchange or luminescence related to the presence of lanthanides in the framework). In heteropolyhedral structures the non-tetrahedral coordination polyhedra (typically octahedra) can host a variety of cations; thus, the frameworks offer a range of crystal-chemical opportunities far wider than in tetrahedral frameworks like zeolites (Rocha & Lin, 2005). This is partly the reason for trying to find new microporous crystalline materials for technological applications.

The $4^15^16^18^2$ silicate sheet has so far only been found in synthetic compounds with the general formula $A_3RESi_6O_{15}\cdot pH_2O$ (A = Na, K, H_3O; RE = rare-earth elements; Haile *et al.*, 1997; Wang *et al.*, 2007). These compounds show luminescence and fast ionic conduction. The closest mineral compounds are those of the sazhinite series {*cf.* sazhinite-(La), $Na_3La[Si_6O_{14}(OH)]\cdot 1.5H_2O$; Càmara *et al.*, 2006}, where the five-rings are missing. We have synthesized and structurally characterized four new silicates containing $4^15^16^18^2$ sheets and the results are reported in this article with a

Table 1
Experimental details.

For all structures: orthorhombic, *Cmm*2, $Z = 4$. Experiments were carried out at 293 K with Mo $K\alpha$ radiation using an Oxford X'Calibur Gemini Ultra diffractometer. Refinement was with 1 restraint. The absolute structure was obtained using Flack (1983).

	TR05	TR06	TR07	TR08
Crystal data				
Chemical formula	$Na_{2.74}K_{0.26}CeSi_6O_{15}\cdot 2.25H_2O$	$Na_{2.72}K_{0.25}LaSi_6O_{15}\cdot 2.25H_2O$	$Na_{3.0}LaSi_6O_{15}\cdot 2.25H_2O$	$Na_{2.74}(H_3O)_{0.26}La_{0.68}Eu_{0.32}Si_6O_{15}\cdot 2.25H_2O$
M_r	662.345	660.16	656.96	660.09
a, b, c (Å)	7.4128 (1), 30.9652 (6), 7.1756 (1)	7.4217 (2), 31.0393 (7), 7.1962 (1)	7.4151 (3), 31.008 (14), 7.1532 (3)	7.3907 (1), 30.8726 (6), 7.1271 (1)
V (Å^3)	1647.08 (5)	1657.75 (6)	1644.43 (12)	1626.19 (4)
θ range (°) for cell measurement	3.1–32.6	3.0–32.7	3.0–29.1	3.1–32.7
μ (mm^{-1})	3.43	3.25	3.20	3.63
Crystal size (mm)	0.18 × 0.05 × 0.04	0.18 × 0.06 × 0.03	0.17 × 0.05 × 0.04	0.15 × 0.05 × 0.04
Data collection				
Absorption correction	Multi-scan	Multi-scan	Multi-scan	Multi-scan
T_{min}, T_{max}	0.886, 1.000	0.743, 1.000	0.688, 1.000	0.913, 1.000
No. of measured, independent and observed $[I_o > 2\sigma(I_o)]$ reflections	26 071, 3182, 2987	22 843, 3158, 3022	7624, 1952, 1896	22 263, 3105, 2877
R_{int}	0.047	0.082	0.053	0.071
Refinement				
$R[F^2 > 2\sigma(F^2)]$, $wR(F^2)$, S	0.033, 0.093, 0.64	0.074, 0.172, 1.38	0.053, 0.150, 1.29	0.051, 0.136, 1.04
No. of reflections	3182	3158	1952	3105
No. of parameters	149	135	140	141
$\Delta\rho_{max}$, $\Delta\rho_{min}$ (e Å^{-3}) and close atoms	2.63 (Ce), −0.75 (Ce)	6.61 (*A*1), −2.07 (*A*1)	5.00 (*A*1), −0.99 (O1)	3.42 (*A*1), −1.84 (*A*1)
Flack (1983) parameter	−0.008 (15)	0.45 (3)	0.07 (3)	0.11 (2)

Computer programs: *CrysAlis CCD* (Oxford Diffraction, 2007*a*), *CrysAlis RED* (Oxford Diffraction, 2007*b*), *SHELXS*86 and *SHELXL*97 (Sheldrick, 2008), *ORTEP* for Windows (Farrugia, 1997), *ATOMS*6.2 (Dowty, 2002), *WinGX* publication routines (Farrugia, 1999).

discussion on the general crystal-chemical features, including the possible occurrence of $(H_3O)^+$ and revisitation of results published by Wang *et al.* (2007).

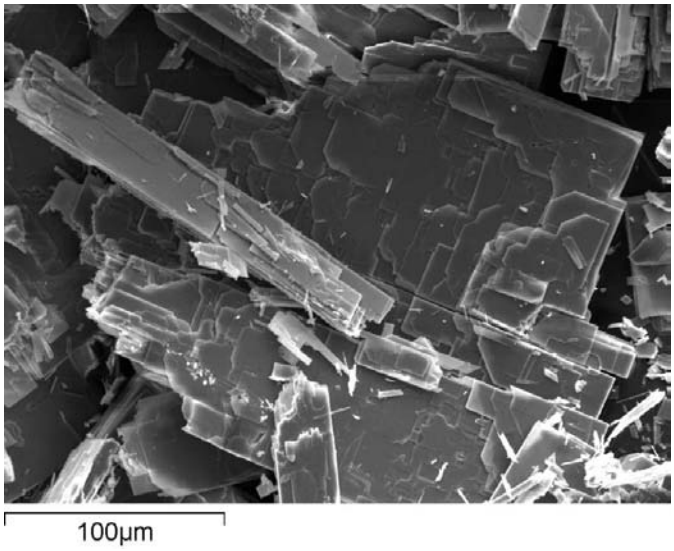

Figure 2
SEM image of TR06 crystals. The other compounds show a similar morphology.

2. Experimental

2.1. Synthesis and identification of the products

The synthesis of the studied compounds was carried out in Teflon-lined autoclaves under hydrothermal conditions at 503 K. At the end of each run, the autoclave was quenched in cold water; the obtained product was filtered, washed at room temperature with distilled water and finally dried at room temperature. In a typical synthesis, an alkaline solution was made by mixing fumed SiO_2 in an NaOH solution; RE salts were then added and the solution thoroughly stirred. These gels with composition $0.8 - x Na_2O{:}x K_2O{:}1.0SiO_2{:}0.05RE_2O_3{:}55H_2O$ were autoclaved under autogenous pressure for 8 d. Aldrich chemicals were used throughout.

Powder X-ray diffraction patterns, collected on a Siemens D5000 diffractometer (Cu $K\alpha$ radiation), revealed high purity products for TR05, TR06 and TR08; in TR07 the presence of a second unknown phase was detected (see Table 1 for TR labels).

Morphological examination (Fig. 2) and semi-quantitative electron-microprobe chemical analyses were carried out on carbon-coated samples by a scanning electron microscope (Stereoscan S360 Cambridge equipped with an Energy 200 Oxford Instruments EDS apparatus; 15 kV accelerating voltage). Quantitative electron-microprobe analyses were performed using a Jeol JXA 8200 Superprobe equipped with a

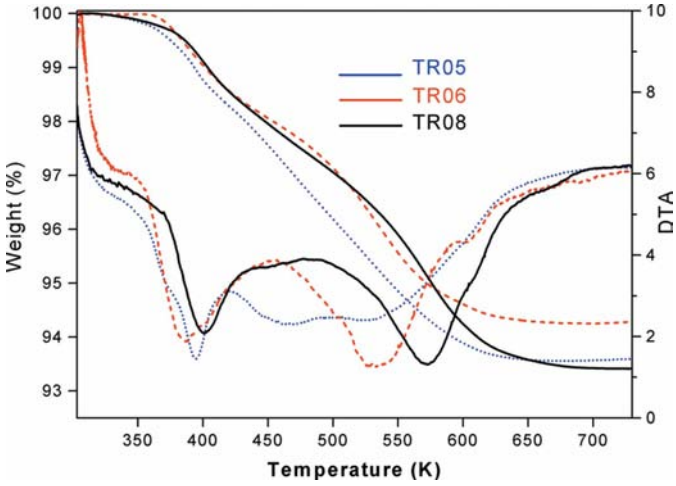

Figure 3
Thermogravimetric curves and their derivatives for TR05, TR06 and TR08.

wavelength-dispersive spectrometer (WDS; operated at 15 kV and 5 nA beam current; 10 µm diameter beam). The subsequent structure determinations lead to the chemical compositions given as the formulae reported in Table 1.

2.2. Thermal analysis

Thermal degradation (Fig. 3) was measured for the pure products (TR05, TR06 and TR08) on approximately 15 mg samples by a TGA Q500 balance (TA Inc.) equipped with an alumina pan placed in a 100 cm^3 min^{-1} nitrogen flow. A heating ramp of 10 K min^{-1} from room temperature up to 1073 K was used.

2.3. Single-crystal diffraction

X-ray single-crystal diffraction data were collected on an Oxford Gemini R Ultra diffractometer equipped with a CCD area detector (50 kV, 40 mA; graphite-monochromated Mo *Kα* radiation). Information on data collection is given in Table 1. Three-dimensional data were integrated and corrected for Lorentz and polarization background effects and absorption using the package *CrysAlis*^{Pro} (Oxford Diffraction, 2007*a*,*b*). The refinement of the cell parameters was based on all measured reflections with $I_o > 20\sigma(I_o)$.

3. Results

3.1. Structure solution and refinement

The crystal structures were solved by direct methods and refined using *SHELXL*97 (Sheldrick, 2008) and the *WinGX* package (Farrugia, 1999); finally they were checked by *PLATON* (Spek, 2009). Information on the refinement is reported in Table 1.[1]

[1] Supplementary data for this paper are available from the IUCr electronic archives (Reference: WH5009). Services for accessing these data are described at the back of the journal.

Table 2
Important bond lengths (Å); O*W* represents the O atoms of the H_2O molecules.

	TR05	TR06	TR07	TR08
†RE—O6	2.346 (4)	2.374 (8)	2.35 (1)	2.315 (7)
RE—O11 × 2	2.384 (3)	2.415 (6)	2.417 (7)	2.377 (6)
RE—O5 × 2	2.424 (3)	2.453 (6)	2.462 (6)	2.417 (5)
RE—O10	2.540 (5)	2.56 (1)	2.57 (1)	2.548 (8)
RE—O9	2.773 (5)	2.77 (1)	2.74 (1)	2.738 (9)
‡*A*1—O11 ×2	2.399 (4)	2.375 (7)	2.358 (8)	2.371 (6)
*A*1—O5 ×2	2.458 (4)	2.474 (6)	2.460 (7)	2.459 (6)
*A*1—O*W*2	2.59 (1)	2.58 (2)	2.51 (2)	2.57 (2)
A—O*W*3 ×2	2.70 (1)	2.76 (3)	2.81 (2)	2.71 (2)
§¶*A*2—O*W*2	2.29 (1)	2.11 (2)	2.28 (2)	2.23 (1)
*A*2—O10	2.447 (5)	2.434 (9)	2.435 (1)	2.419 (9)
*A*2—O3	2.568 (7)	2.55 (2)	2.41 (2)	2.42 (1)
*A*2—O10	2.582 (6)	2.57 (1)	2.35 (1)	2.419 (9)
A—O11	2.975 (6)	2.99 (1)	2.88 (1)	2.90 (1)
*A*2—O1	3.066 (7)	3.11 (1)	3.15 (2)	3.10 (1)
*A*2—O*W*2	3.12 (1)	2.92 (2)	3.12 (2)	3.10 (1)
¶††*A*3—*A*3′	2.220 (1)	2.29 (3)	2.33 (3)	2.32 (2)
*A*3—O*W*1	2.259 (8)	2.25 (1)	2.25 (1)	2.248 (9)
*A*3—O*W*3	2.42 (1)	2.46 (2)	2.47 (2)	2.44 (2)
*A*3—O6	2.569 (7)	2.54 (1)	2.52 (1)	2.54 (1)
*A*3—O5	2.578 (7)	2.56 (2)	2.54 (1)	2.54 (1)
*A*3—O8	2.652 (7)	2.57 (2)	2.62 (1)	2.60 (1)
*A*3—O4	3.029 (8)	3.04 (2)	3.06 (2)	3.03 (1)
*A*3—O*W*3	3.11 (1)	3.13 (3)	3.07 (2)	3.10 (2)
Si1—O10	1.586 (5)	1.62 (1)	1.62 (1)	1.607 (9)
Si1—O1 ×2	1.603 (3)	1.626 (7)	1.618 (9)	1.623 (6)
Si1—O9	1.640 (4)	1.652 (9)	1.644 (9)	1.650 (8)
Si2—O6	1.582 (5)	1.583 (9)	1.59 (1)	1.572 (8)
Si2—O8 ×2	1.628 (3)	1.615 (6)	1.600 (7)	1.614 (5)
Si2—O9	1.641 (5)	1.632 (9)	1.65 (1)	1.645 (8)
Si3—O5	1.578 (3)	1.574 (6)	1.566 (7)	1.567 (5)
Si3—O7	1.626 (2)	1.625 (4)	1.630 (4)	1.629 (3)
Si3—O8	1.629 (3)	1.636 (6)	1.642 (7)	1.645 (6)
Si3—O4	1.630 (2)	1.626 (6)	1.624 (4)	1.625 (3)
Si4—O11	1.578 (4)	1.554 (7)	1.562 (8)	1.566 (6)
Si4—O1	1.630 (4)	1.614 (9)	1.62 (1)	1.613 (7)
Si4—O2	1.626 (2)	1.628 (4)	1.629 (4)	1.624 (3)
Si4—O3	1.638 (2)	1.638 (4)	1.647 (5)	1.644 (4)
¶O*W*1—O6	2.901 (7)	2.91 (1)	2.92 (1)	2.92 (1)
O*W*1—O4	3.06 (2)	3.08 (3)	3.06 (3)	3.05 (2)
‡‡O*W*2—O2	3.05 (2)	3.06 (3)	3.07 (3)	3.08 (2)
O*W*2—O11	3.17 (1)	3.03 (2)	3.08 (2)	3.11 (2)
¶O*W*3—O5	2.81 (1)	2.83 (3)	2.77 (3)	2.77 (2)
O*W*3—O8	2.98 (1)	2.96 (3)	2.97 (3)	2.97 (2)

† RE = Ce (TR05), La (TR06 and TR08), $La_{0.68\%}Eu_{0.32\%}$ (TR08). ‡ *A*1 = Na (TR06, TR07 and TR08), $Na_{0.72\%}K_{0.28\%}$ (TR06). § *A*2 = Na (TR06, TR07 and TR08), $Na_{0.74\%}K_{0.26\%}$ (TR05). ¶ 50% occupancy. †† *A*3 = Na (TR05, TR06 and TR07), $Na_{0.74\%}(H_3O)_{0.26\%}$ (TR08). ‡‡ In TR06 O*W*2 is on a 50% occupied general position that is close to the (100) mirror plane.

Except for TR05 where the diffraction data were collected on a single crystal, the other three compounds were composed of crystals affected by {001} twinning by merohedry. The volume of the smaller individual is given in the line 'Flack parameter' of Table 1; in TR06 the volumes of the two individuals are almost equal, thus a detwinning procedure cannot be applied (*cf.* Nespolo & Ferraris, 2000) and the absolute structure remains undetermined. A mixed occupancy of sites

(Table 2) has been determined by using constraints *via* the FVAR procedure of *SHELX*.

The presence of heavy atoms, twinning, partial occupancy of sites and mixed occupancy for $(H_3O)^+$ in TR08 (Table 2) prevented the localization of the H atoms but, as discussed in §4.2, a hydrogen-bonding scheme can be established. For the same reasons the O*W* O atoms, except for O*W*1 in TR06, could only be refined isotropically. Other atoms that could not be anisotropically refined are: O1 (TR06, TR07), O5 (TR06), *A*1 (TR06, TR07, TR08), *A*2 (the minor K component in TR05), *A*3 (TR05, TR06, TR08) and RE (TR08).

The largest residual peaks are close to either heavy RE atoms or to atoms that, likely because of some disorder, could not be anisotropically refined (Table 1). Disorder and mixed occupancy are also responsible for the lack of convergence of the isotropic atomic displacement parameter of *A*1 in TR06 and *A*3 in TR08 (shift/error > 1).

4. Structural aspects

The structures of TR05, TR06, TR07 and TR08 are isotypic; Fig. 4 shows views of the crystal structure of TR05 that is representative of the other three compounds. Table 2 reports important bond lengths of the studied structures.

4.1. The heteropolyhedral framework

In TR05, TR06, TR07 and TR08 strongly corrugated $4^1.5^1.6^1.8^2$ sheets (Fig. 1*g*) are periodically repeated along [001] and interconnected by seven-coordinated RE polyhedra (*P*7) to form a heteropolyhedral framework (Fig. 4). *P*7 shares its O9—O10 edge with the Si1 tetrahedron; to minimize cation repulsion, O9—O10 (∼ 2.54 Å) is the shortest tetrahedral distance in the structure. The framework is crossed by three systems of ellipsoidal eight-rings that stack either parallel (*R*1 and *R*2, along [100]) or perpendicular (*R*3, along [001]) to the silicate sheets. The formation of *R*1 and *R*2 is a consequence of the heteropolyhedral structure and each ring consists of four tetrahedra and two *P*7. *R*3, instead, corresponds to the eight-ring of the $4^1.5^1.6^1.8^2$ sheet. The stacking of both *R*1 and *R*2 produces two channels (*ch*1 and *ch*2, respectively), whose effective channel widths (e.c.w.), calculated according to McCusker *et al.* (2003) by subtracting the ionic diameter of O^{2-} (2.7 Å) from the shortest and the longest O···O distance across each channel, are ∼ 4.5 × 2.8 and 4.5 × 1 Å for *ch*1 and *ch*2, respectively. The stacking of *R*3 is intercalated by *P*7 polyhedra: thus, the e.c.w. of 4.7 × 2 Å that should be allowed for this *ch*3 channel by the silicate rings alone is drastically reduced to ∼ 2 × 2 Å. Actually, the four-, five- and six-rings of the $4^1.5^1.6^1.8^2$ sheet also define channels along [001]; however, the e.c.w.s of these channels are too small to contribute to the microporosity of the structure.

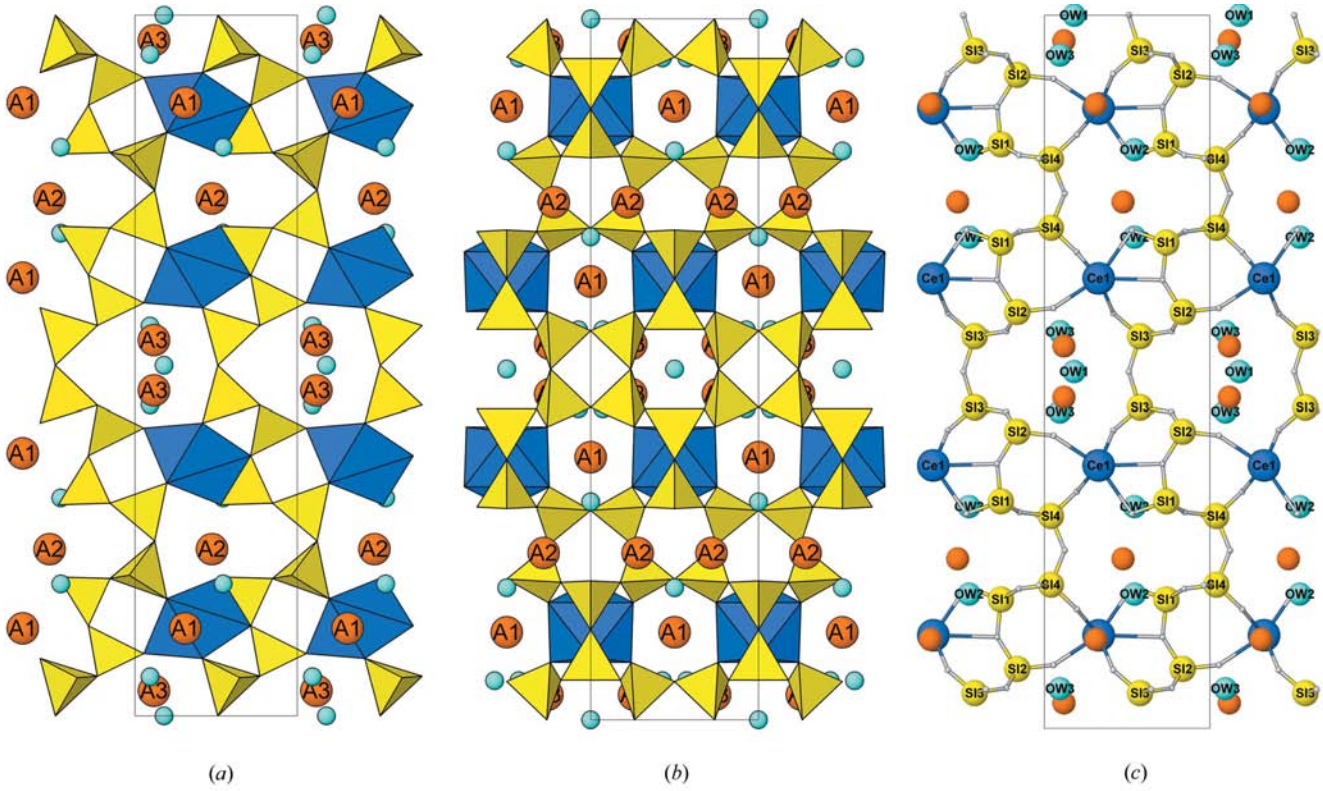

Figure 4
Crystal structure of TR05 seen (*a*) along [100], parallel to the silicate sheets, and (*b*) along [001], perpendicular to the sheets. In (*c*), with the same orientation of (*a*), labelling of Si, Ce and O*W* atoms is shown. Labelling of the *A* sites (see Table 2 for composition) is shown both in (*a*) and (*b*); Ce polyhedra are shown in blue. The vertical axis is **c**.

As expected for bond-valence reasons, the shortest Si—O bond lengths (~ 1.58 Å) correspond to the O atoms (O5, O6, O10 and O11) bonded to only one Si atom; the same O atoms also form a bond with the RE atom. O9 is the only O atom bonded at the same time to two Si atoms and one RE atom: it shows the longest Si—O bond length (~ 1.64 Å). Except O9, all O and O*W* atoms are coordinated to one or more alkali ions (Table 2).

4.2. The channel content and $(H_3O)^+$ occurrence

The three crystallographically independent H_2O molecules occur within *ch*1 (O*W*1 and O*W*3) and *ch*2 (O*W*2) (Fig. 4). The occupancy of both O*W*1 and O*W*3 sites is 50%; partial occupancy for O*W*3 allows local avoidance of a short *A*3···O*W*3 ~ 1.4 Å distance. The O*W*2 site is 50% occupied only in TR06, where it occurs in a general position close to the (100) mirror plane where it lies exactly in TR05. As stated in §3.1, the position of the H atoms has not been determined. However, on the basis of the O*W*···O contacts (Table 2) and the O···O*W*···O angles it is possible to establish that O*W*1, O*W*2 and O*W*3 are donors of weak hydrogen bonds (Chiari & Ferraris, 1982) to the following acceptors, in the order: O6 and O4 (O6···O*W*1···O4 ~ 104°), O2 and O11 (O2···O*W*2···O11 ≃ 143°), O5 and O8 (O5···O*W*3···O8 ≃ 109°).

The *A*1, *A*2 and *A*3 alkaline sites occur within the *ch*3, *ch*2 and *ch*1 channels, respectively. *A*2 and *A*3 are only 50% occupied to avoid short distances, either between crystallographically equivalent positions (*A*2···*A*2′ ~ 0.9 Å; *A*3···*A*3′ ~ 2.3 Å) or between independent positions (*A*3···O*W*3 ~1.4 Å). For all *A* sites the coordination number is seven, but four (*A*2 site) and five (*A*3 site) *A*···O distances are by far shorter than the remaining distances (Table 2). About 0.3 atoms per formula unit (a.p.f.u.) of K^+ replace Na^+ in TR05 and TR06. However, K^+ enters the *A*2 site in TR05 and *A*1 in TR06. The different behaviour is likely connected to the ionic radius of Ce^{3+} (TR05) and La^{3+} (TR06), such that their coordination polyhedra differently interact with *A*1 and *A*2: the average bond length in the La polyhedron is 2.49 Å in TR06 and TR07, whereas in the Ce polyhedron (TR05) it is slightly smaller (2.47 Å).

In TR08 the refinement of the Na against O content at *A*3 shows that 26% of this site is occupied by an O atom, in agreement with the chemical analysis that indicates less than 3 Na a.p.f.u. If this O were an H_2O molecule, the charge balance would have to be provided by a very improbable higher valence of the RE (Eu and La); a more realistic hypothesis is that the missing 26% Na is replaced by $(H_3O)^+$. Although a high contribution of the Eu fluorescence unfortunately prevented the acquisition of a Raman spectrum which could provide further evidence, this latter hypothesis is supported by the following considerations.

*A*3 and three O atoms (O5, O6, O8), at an *A*3···O distance ≤ 2.6 Å (Table 2), are the vertices of a distorted tetrahedron, a typical situation observed for $(H_3O)^+$ (*e.g.* Catti & Ibberson, 2002; Alonso & Turrillas, 2005). Locally a configuration suitable for hosting hydronium occurs when the 50% occupied O*W*1 and O*W*3 sites are empty: in particular, the distance *A*3···O*W*1 = 2.25 Å is incompatible with *A*3 = $(H_3O)^+$, but is suitable for *A*3 = Na^+.

Thermal analysis (Fig. 3) shows that the loss of H_2O occurs in two main stages as shown by two broad main peaks in the derivative curves. Only the donors of the weaker hydrogen bonds, O*W*1 and O*W*2, should contribute to the first stage. O*W*3 is instead a donor of stronger hydrogen bonds and should contribute (only) to the second stage of H_2O loss. In spite of the very similar O*W*3···O distances in the four studied compounds (Table 2), the second peak of the derivative curve is at a temperature of 570 K in TR08, namely ~ 320 K higher than in TR05 and TR06. Taking into account also that the total weight loss of TR08 is higher (6.6%) than in TR05 and TR06, one can conclude that the strongly hydrogen-bonded 26% of $(H_3O)^+$ present at *A*3 in TR08 contributes to the final stage of weight loss. For comparison, the calculated weight loss for TR08 is either 6.1 or 8.8% including or excluding $(H_3O)^+$, respectively.

5. Discussion

Wang *et al.* (2007) studied a synthetic silicate ($Na_{2.4}CeSi_6O_{15}\cdot 2.6H_2O$, a = 7.4165, b = 30.966, c = 7.1539 Å, Z = 4, *Cmm*2) similar to TR05. On the basis of photon spectroscopy and magnetic susceptibility measurements, these authors concluded that the studied silicate contains Ce mixed-valence ions. According to their description of the structure, Wang *et al.* (2007) placed Na only in the sites that in TR05 are labelled *A*1 and *A*2; at the same time they placed H_2O in *A*3, O*W*1 and O*W*2 sites and left empty the site labelled O*W*3 in TR05. Consequently, Wang *et al.* (2007) deduced from the structural data the following formula for their compound: $Na_{2.4}Ce^{3+}_{0.4}Ce^{4+}_{0.6}Si_6O_{15}\cdot 2.6H_2O$, but no chemical analyses were included to support this interpretation.

Taking into account that, as discussed above, the maximum occupancy of *A*2 is 50%, we conclude that the content of 2.4 Na a.p.f.u. deduced by Wang *et al.* (2007) from their structural data is incorrect and must be reduced to 2 a.p.f.u.

To summarize two hypotheses can be proposed to explain the results of Wang *et al.* (2007); in both cases Na^+ may be partially substituted by $(H_3O)^+$.

The presence of Ce mixed-valence ions is correct: In this case, to match the given Ce^{3+}/Ce^{4+} ratio a missing 0.4 Na a.p.f.u. must occur either in a site attributed to H_2O or in the empty O*W*3 site (TR05 labelling).

Only Ce^{3+} occurs, as in TR05: In this second case, either a total of 3 Na a.p.f.u must occur or some missing Na^+ is compensated by $(H_3O)^+$, as in TR08.

6. Conclusions

The structural analysis of four synthetic heteropolyhedral microporous silicates, with the general formula $A_3RESi_6O_{15}\cdot 2.25H_2O$ (A = Na, K, H_3O; RE = La, Ce, Eu) and

based on $4^1 5^1 6^1 8^2$ tetrahedral sheets, allows the following general conclusions:

(i) The complex $RESi_6O_{15}$ anion is charge-balanced by alkaline and $(H_3O)^+$ cations; the results published by Wang *et al.* (2007) for the compound with RE = Ce, assuming the occurrence of Ce mixed-valence ions, have been reinterpreted.

(ii) More than one type of RE may occur in the same crystallographic site.

(iii) More than one type of alkaline cation may occur in the same *A* site; the *A* site with composite occupancy may be different in different compounds, likely depending on the nature of the RE.

(iv) The configuration of one *A* site is suitable to host both alkalis and $(H_3O)^+$; the latter donates three short hydrogen bonds, thus assuming a typical tetrahedral configuration.

Property (ii) can be exploited to produce materials fluorescing at different wavelengths. Property (iii) supports the experimentally proven (Wang *et al.*, 2007) cation exchange capability and ionic conduction of the described structure type.

This work was financially supported by MIUR [Roma, project PRIN 2007 'Compositional and structural complexity in minerals (crystal chemistry, microstructures, modularity, modulations): analysis and applications']. The constructive comments of an anonymous reviewer and of the co-editor T. J. White helped to improve the text.

References

Alonso, J. A. & Turrillas, X. (2005). *Dalton Trans.* pp. 865–867.
Ananias, D., Kostova, M., Paz, F. A. A., Neto, A. N. C., De Moura, R. T., Malta, O. L., Carlos, L. D. & Rocha, J. (2009). *J. Am. Chem. Soc.* **131**, 8620–8626.
Artioli, G. & Galli, E. (1994). *Mater. Sci. Forum*, **166–169**, 647–652.
Brauner, K. & Preisinger, A. (1956). *Tsch. Mineral. Petrogr. Mitt.* **6**, 120–140.
Cadoni, M. & Ferraris, G. (2009). *Eur. J. Mineral.* **21**, 485–493.
Cadoni, M. & Ferraris, G. (2010). *Acta Cryst.* 151–157.
Càmara, F., Ottolini, L., Devouard, B., Garvie, L. A. J. & Hawthorne, F. C. (2006). *Mineral. Mag.* **70**, 405–418.
Catti, M. & Ibberson, R. M. (2002). *J. Phys. Chem. B*, **106**, 1916–1921.
Chiari, G. & Ferraris, G. (1982). *Acta Cryst.* B**38**, 2331–2341.
Dowty, E. (2002). *ATOMS*, Version 6.2. Shape Software, Kingsport, Tennessee, USA.
Farrugia, L. J. (1997). *J. Appl. Cryst.* **30**, 565.
Farrugia, L. J. (1999). *J. Appl. Cryst.* **32**, 837–838.
Ferraris, G., Khomyakov, A. P., Belluso, E. & Soboleva, S. V. (1998). *Eur. J. Mineral.* **10**, 865–874.
Ferraris, G., Makovicky, E. & Merlino, S. (2008). *Crystallography of Modular Materials.* Oxford University Press.
Ferraris, G. & Merlino, S. (2005). Editors. *Micro- and Mesoporous Mineral Phases.* Washington DC: Mineralogical Society of America, Geochemical Society.
Flack, H. D. (1983). *Acta Cryst.* A**39**, 876–881.
Grice, J. D. & Hawthorne, F. C. (2002). *Can. Mineral.* **40**, 971–980.
Haile, S. M. & Wuensch, B. J. (1997). *Am. Mineral.* **82**, 1141–1149.
Haile, S. M., Wuensch, B. J., Laudise, R. A. & Maier, J. (1997). *Acta Cryst.* B**53**, 7–17.
Krivovichev, S. V. (2009). *Structural Crystallography of Inorganic Oxysalts.* Oxford University Press.
Liebau, F. (1985). *Structural Chemistry of Silicates. Structure, Bonding and Classification.* Berlin: Springer.
McCusker, L. B., Liebau, F. & Engelhardt, G. (2003). *Microporous Mesoporous Mater.* **58**, 3–13.
Nespolo, M. & Ferraris, G. (2000). *Z. Kristallogr.* **215**, 77–81.
Oxford Diffraction (2007*a*). *CrysAlis CCD.* Oxford Diffraction Ltd, Abingdon, Oxfordshire, England.
Oxford Diffraction (2007*b*). *CrysAlis RED.* Oxford Diffraction Ltd, Abingdon, Oxfordshire, England.
Prinz, S., Sparta, K. M. & Roth, G. (2008). *Acta Cryst.* C**64**, i27–i29.
Rocha, J. & Lin, Z. (2005). *Rev. Mineral. Geochem.* **57**, 173–201.
Sheldrick, G. M. (2008). *Acta Cryst.* A**64**, 112–122.
Spek, A. L. (2009). *Acta Cryst.* D**65**, 148–155.
Wang, G., Yan, W., Chen, P., Wang, X., Qian, K., Su, T. & Yu, J. (2007). *Microporous Mesoporous Mater.* **105**, 58–64.
Wang, X., Liu, L. & Jacobson, A. J. (2003). *Angew. Chem.* **115**, 2090–2093.
Watanabe, I. & Kawahara, A. (1993). *Acta Cryst.* C**49**, 854–856.